Observation of a new charged charmonium-like state in $\bar{B}^0 \to J/\psi K^- \pi^+$ decays

K. Chilikin,[22] R. Mizuk,[22, 36] I. Adachi,[14, 10] H. Aihara,[60] S. Al Said,[55, 26] K. Arinstein,[4] D. M. Asner,[47] V. Aulchenko,[4] T. Aushev,[22] R. Ayad,[55] T. Aziz,[56] A. M. Bakich,[54] V. Bansal,[47] A. Bondar,[4] G. Bonvicini,[65] A. Bozek,[44] M. Bračko,[33, 23] T. E. Browder,[13] D. Červenkov,[5] V. Chekelian,[34] A. Chen,[41] B. G. Cheon,[12] R. Chistov,[22] K. Cho,[27] V. Chobanova,[34] S.-K. Choi,[11] Y. Choi,[53] D. Cinabro,[65] M. Danilov,[22, 36] Z. Doležal,[5] Z. Drásal,[5] A. Drutskoy,[22, 36] K. Dutta,[16] S. Eidelman,[4] D. Epifanov,[60] H. Farhat,[65] J. E. Fast,[47] T. Ferber,[8] O. Frost,[8] V. Gaur,[56] N. Gabyshev,[4] S. Ganguly,[65] A. Garmash,[4] R. Gillard,[65] Y. M. Goh,[12] B. Golob,[31, 23] O. Grzymkowska,[44] J. Haba,[14, 10] T. Hara,[14, 10] K. Hayasaka,[39] H. Hayashii,[40] X. H. He,[48] W.-S. Hou,[43] M. Huschle,[25] H. J. Hyun,[29] A. Ishikawa,[59] R. Itoh,[14, 10] Y. Iwasaki,[14] I. Jaegle,[13] K. K. Joo,[6] T. Julius,[35] T. Kawasaki,[45] C. Kiesling,[34] D. Y. Kim,[52] H. J. Kim,[29] J. H. Kim,[27] M. J. Kim,[29] Y. J. Kim,[27] K. Kinoshita,[7] B. R. Ko,[28] S. Korpar,[33, 23] P. Križan,[31, 23] P. Krokovny,[4] T. Kuhr,[25] A. Kuzmin,[4] Y.-J. Kwon,[66] J. S. Lange,[9] Y. Li,[64] L. Li Gioi,[34] J. Libby,[17] Y. Liu,[7] D. Liventsev,[14] P. Lukin,[4] K. Miyabayashi,[40] H. Miyata,[45] G. B. Mohanty,[56] A. Moll,[34, 57] T. Mori,[38] R. Mussa,[21] E. Nakano,[46] M. Nakao,[14, 10] T. Nanut,[23] Z. Natkaniec,[44] E. Nedelkovska,[34] N. K. Nisar,[56] S. Nishida,[14, 10] S. Ogawa,[58] S. Okuno,[24] P. Pakhlov,[22, 36] G. Pakhlova,[22] C. W. Park,[53] H. Park,[29] T. K. Pedlar,[32] M. Petrič,[23] L. E. Piilonen,[64] E. Ribežl,[23] M. Ritter,[34] A. Rostomyan,[8] Y. Sakai,[14, 10] S. Sandilya,[56] L. Santelj,[23] T. Sanuki,[59] Y. Sato,[59] V. Savinov,[49] O. Schneider,[30] G. Schnell,[1, 15] C. Schwanda,[19] O. Seon,[38] V. Shebalin,[4] C. P. Shen,[2] T.-A. Shibata,[61] J.-G. Shiu,[43] B. Shwartz,[4] A. Sibidanov,[54] F. Simon,[34, 57] Y.-S. Sohn,[66] A. Sokolov,[20] E. Solovieva,[22] M. Starič,[23] M. Steder,[8] K. Sumisawa,[14, 10] T. Sumiyoshi,[62] U. Tamponi,[21, 63] K. Tanida,[51] G. Tatishvili,[47] Y. Teramoto,[46] F. Thorne,[19] K. Trabelsi,[14, 10] M. Uchida,[61] S. Uehara,[14, 10] T. Uglov,[22, 37] Y. Unno,[12] S. Uno,[14, 10] P. Urquijo,[3] C. Van Hulse,[1] P. Vanhoefer,[34] G. Varner,[13] A. Vinokurova,[4] M. N. Wagner,[9] C. H. Wang,[42] M.-Z. Wang,[43] P. Wang,[18] X. L. Wang,[64] Y. Watanabe,[24] S. Wehle,[8] K. M. Williams,[64] E. Won,[28] J. Yamaoka,[47] S. Yashchenko,[8] Z. P. Zhang,[50] V. Zhilich,[4] V. Zhulanov,[4] and A. Zupanc[23]

(The Belle Collaboration)

[1] University of the Basque Country UPV/EHU, 48080 Bilbao
[2] Beihang University, Beijing 100191
[3] University of Bonn, 53115 Bonn
[4] Budker Institute of Nuclear Physics SB RAS and Novosibirsk State University, Novosibirsk 630090
[5] Faculty of Mathematics and Physics, Charles University, 121 16 Prague
[6] Chonnam National University, Kwangju 660-701
[7] University of Cincinnati, Cincinnati, Ohio 45221
[8] Deutsches Elektronen–Synchrotron, 22607 Hamburg
[9] Justus-Liebig-Universität Gießen, 35392 Gießen
[10] The Graduate University for Advanced Studies, Hayama 240-0193
[11] Gyeongsang National University, Chinju 660-701
[12] Hanyang University, Seoul 133-791
[13] University of Hawaii, Honolulu, Hawaii 96822
[14] High Energy Accelerator Research Organization (KEK), Tsukuba 305-0801
[15] IKERBASQUE, Basque Foundation for Science, 48011 Bilbao
[16] Indian Institute of Technology Guwahati, Assam 781039
[17] Indian Institute of Technology Madras, Chennai 600036
[18] Institute of High Energy Physics, Chinese Academy of Sciences, Beijing 100049
[19] Institute of High Energy Physics, Vienna 1050
[20] Institute for High Energy Physics, Protvino 142281
[21] INFN - Sezione di Torino, 10125 Torino
[22] Institute for Theoretical and Experimental Physics, Moscow 117218
[23] J. Stefan Institute, 1000 Ljubljana
[24] Kanagawa University, Yokohama 221-8686
[25] Institut für Experimentelle Kernphysik, Karlsruher Institut für Technologie, 76131 Karlsruhe
[26] Department of Physics, Faculty of Science, King Abdulaziz University, Jeddah 21589
[27] Korea Institute of Science and Technology Information, Daejeon 305-806
[28] Korea University, Seoul 136-713
[29] Kyungpook National University, Daegu 702-701
[30] École Polytechnique Fédérale de Lausanne (EPFL), Lausanne 1015
[31] Faculty of Mathematics and Physics, University of Ljubljana, 1000 Ljubljana
[32] Luther College, Decorah, Iowa 52101
[33] University of Maribor, 2000 Maribor
[34] Max-Planck-Institut für Physik, 80805 München

[35]School of Physics, University of Melbourne, Victoria 3010
[36]Moscow Physical Engineering Institute, Moscow 115409
[37]Moscow Institute of Physics and Technology, Moscow Region 141700
[38]Graduate School of Science, Nagoya University, Nagoya 464-8602
[39]Kobayashi-Maskawa Institute, Nagoya University, Nagoya 464-8602
[40]Nara Women's University, Nara 630-8506
[41]National Central University, Chung-li 32054
[42]National United University, Miao Li 36003
[43]Department of Physics, National Taiwan University, Taipei 10617
[44]H. Niewodniczanski Institute of Nuclear Physics, Krakow 31-342
[45]Niigata University, Niigata 950-2181
[46]Osaka City University, Osaka 558-8585
[47]Pacific Northwest National Laboratory, Richland, Washington 99352
[48]Peking University, Beijing 100871
[49]University of Pittsburgh, Pittsburgh, Pennsylvania 15260
[50]University of Science and Technology of China, Hefei 230026
[51]Seoul National University, Seoul 151-742
[52]Soongsil University, Seoul 156-743
[53]Sungkyunkwan University, Suwon 440-746
[54]School of Physics, University of Sydney, NSW 2006
[55]Department of Physics, Faculty of Science, University of Tabuk, Tabuk 71451
[56]Tata Institute of Fundamental Research, Mumbai 400005
[57]Excellence Cluster Universe, Technische Universität München, 85748 Garching
[58]Toho University, Funabashi 274-8510
[59]Tohoku University, Sendai 980-8578
[60]Department of Physics, University of Tokyo, Tokyo 113-0033
[61]Tokyo Institute of Technology, Tokyo 152-8550
[62]Tokyo Metropolitan University, Tokyo 192-0397
[63]University of Torino, 10124 Torino
[64]CNP, Virginia Polytechnic Institute and State University, Blacksburg, Virginia 24061
[65]Wayne State University, Detroit, Michigan 48202
[66]Yonsei University, Seoul 120-749

We present the results of an amplitude analysis of $\bar{B}^0 \to J/\psi K^- \pi^+$ decays. A new charged charmonium-like state $Z_c(4200)^+$ decaying to $J/\psi \pi^+$ is observed with a significance of 6.2σ. The mass and width of the $Z_c(4200)^+$ are 4196^{+31+17}_{-29-13} MeV/c^2 and $370^{+70+70}_{-70-132}$ MeV, respectively; the preferred assignment of the quantum numbers is $J^P = 1^+$. In addition, we find evidence for $Z_c(4430)^+ \to J/\psi \pi^+$. The analysis is based on a 711 fb^{-1} data sample collected by the Belle detector at the asymmetric-energy e^+e^- collider KEKB.

I. INTRODUCTION

Recently, a number of new states containing a $c\bar{c}$ quark pair have been observed, many of which are not well described by the quark model [1–3]. Among these states are charged charmonium-like state candidates with a minimal quark content that is necessarily exotic: $|c\bar{c}u\bar{d}\rangle$. The first of these states, the $Z_c(4430)^+$, was observed by the Belle Collaboration in the $\psi(2S)\pi^+$ invariant mass spectrum in $\bar{B}^0 \to \psi(2S)K^- \pi^+$ decays [4–6]. Two other states, the $Z_c(4050)^+$ and $Z_c(4250)^+$, were observed by Belle in the $\chi_{c1}\pi^+$ invariant mass spectrum in $\bar{B}^0 \to \chi_{c1}K^- \pi^+$ decays [7]. The BaBar Collaboration searched for these states [8, 9] but did not confirm them. However, recently, the LHCb collaboration confirmed the Belle observation of the $Z_c(4430)^+$ with overwhelming ($> 14\sigma$) significance [10]. The BESIII and Belle Collaborations observed the $Z_c(3900)^\pm$ in the $J/\psi\pi^\pm$ invariant mass spectrum in $Y(4260) \to J/\psi\pi^+\pi^-$

decays [11, 12]. The charged $Z_c(3900)^\pm$ was also observed in CLEO data [13]; in this analysis, evidence for the neutral $Z_c(3900)^0$ was also found. The $Z_c(3885)^\pm$, which is likely to be the same state, was observed by the BESIII Collaboration in $e^+e^- \to (D\bar{D}^*)^\pm\pi^\mp$ [14]. Also, the BESIII Collaboration observed the $Z_c(4020)^\pm$ in the $h_c\pi^\pm$ invariant mass spectrum in $e^+e^- \to h_c\pi^+\pi^-$ [16]. Finally, the $Z_c(4025)^\pm$ was observed by the BESIII Collaboration in $e^+e^- \to (D^*\bar{D}^*)^\pm\pi^\mp$ [15].

Here we present the results of a full amplitude analysis of the decay $\bar{B}^0 \to J/\psi K^- \pi^+$, with $J/\psi \to \mu^+\mu^-$ or $J/\psi \to e^+e^-$. The analysis is similar to the Belle study of $\bar{B}^0 \to \psi(2S)K^- \pi^+$ [6]. It is performed using a 711 fb^{-1} data sample collected by the Belle detector at the KEKB asymmetric-energy e^+e^- collider [17]. The data sample was collected at the $\Upsilon(4S)$ resonance and contains 772×10^6 $B\bar{B}$ pairs.

II. THE BELLE DETECTOR

The Belle detector is a large-solid-angle magnetic spectrometer that consists of a silicon vertex detector (SVD), a 50-layer central drift chamber (CDC), an array of aerogel threshold Cherenkov counters (ACC), a barrel-like arrangement of time-of-flight scintillation counters (TOF), and an electromagnetic calorimeter comprised of CsI(Tl) crystals (ECL) located inside a superconducting solenoid coil that provides a 1.5 T magnetic field. An iron flux-return located outside of the coil is instrumented to detect K_L^0 mesons and to identify muons (KLM). The detector is described in detail elsewhere [18]. Two inner detector configurations were used. A 2.0 cm beampipe and a 3-layer silicon vertex detector were used for the first sample of 155 fb^{-1}, while a 1.5 cm beampipe, a 4-layer silicon detector and a small-cell inner drift chamber were used to record the remaining 556 fb^{-1}[19].

We use a GEANT-based Monte Carlo (MC) simulation [20] to model the response of the detector, identify potential backgrounds and determine the acceptance. The MC simulation includes run-dependent detector performance variations and background conditions. Signal MC events are generated with EvtGen [21] in proportion to the relative luminosities of the different running periods.

III. EVENT SELECTION

We select events of the type $\bar{B}^0 \to J/\psi K^- \pi^+$ (where inclusion of charge-conjugate modes is always implied), with the J/ψ meson reconstructed via its e^+e^- and $\mu^+\mu^-$ decay channels. The selection procedure is identical to Ref. [6] with the replacement of the $\psi(2S)$ by the J/ψ.

All tracks are required to originate from the interaction region, $dr < 0.2$ cm and $|dz| < 2$ cm, where dr and dz are the cylindrical coordinates (the radial distance and longitudinal position, respectively, with the z axis of the reference frame antiparallel to the positron beam axis and the origin being the run-dependent mean interaction point) of the point of closest approach of the track to the z axis in the interaction region. Charged π and K mesons are identified using likelihood ratios $R_{\pi/K} = \mathcal{L}_\pi/(\mathcal{L}_\pi + \mathcal{L}_K)$ and $R_{K/\pi} = \mathcal{L}_K/(\mathcal{L}_\pi + \mathcal{L}_K)$, where $\mathcal{L}_\pi$ and $\mathcal{L}_K$ are likelihoods for π and K, respectively, that are calculated from the time-of-flight information from the TOF, the number of photoelectrons from the ACC and dE/dx measurements in the CDC. We require $R_{\pi/K} > 0.6$ for π candidates and $R_{K/\pi} > 0.6$ for K candidates. The K identification efficiency is typically 90% and the misidentification probability is about 10%. Muons are identified by their range and transverse scattering in the KLM. Electrons are identified by the presence of a matching electromagnetic shower in the ECL. An electron veto is imposed on π and K candidates.

For $J/\psi \to e^+e^-$ candidates, we collect bremsstrahlung radiation by including photons that have energies greater than 30 MeV and are within 50 mrad of the lepton direction in the calculation of the J/ψ invariant mass. We require $|M(\ell^+\ell^-) - m_{J/\psi}| < 60$ MeV/c^2, where ℓ is either μ or e. We perform a mass-constrained fit to the J/ψ candidates. The data from e^+e^- and $\mu^+\mu^-$ channels are combined since both channels have the same angular distribution.

The beam-energy-constrained mass of the B meson is defined as $M_{\rm bc} = \sqrt{E_{\rm beam}^2 - (\sum_i \vec{p}_i)^2}$, where $E_{\rm beam}$ is the beam energy in the center-of-mass frame and $\vec{p}_i$ are the momenta of the decay products in the same frame. We require $|M_{\rm bc} - m_B| < 7$ MeV/c^2, where m_B is the B^0 mass [22]. A mass-constrained fit is applied to the B meson candidates.

IV. EVENT DISTRIBUTIONS AND SIGNAL YIELD

The difference between the reconstructed energy and the beam energy $\Delta E = \sum_i E_i - E_{\rm beam}$, where E_i are energies of the $\bar{B}^0$ decay products in the center-of-mass frame, is used to identify the signal. The signal region is defined as $|\Delta E| < 20$ MeV, and the sidebands are defined as 40 MeV $< |\Delta E| < 80$ MeV. The ΔE distribution with marked signal and sideband regions is shown in Fig. 1.
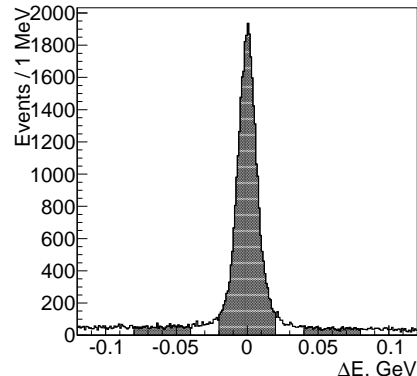

FIG. 1. The ΔE distribution; the signal and sideband regions are hatched.

To determine the signal and background event yields, we perform a binned maximum likelihood fit of the ΔE distribution that is modeled by the sum of two Gaussian functions to represent signal and a second-order polynomial for the background. The total number of events in the signal region is 31 774 and the number of signal events in the signal region is $29\,990 \pm 190 \pm 50$ (here and elsewhere, the first uncertainty is statistical and the second is systematic). The systematic error is estimated by changing the ΔE fit interval and the order of the polynomial.

The Dalitz plot for the signal region is shown in

Fig. 2(a). The most prominent features are the vertical bands due to the production of intermediate $K^*(892)$ and $K_2^*(1430)$ resonances. The Dalitz plot for the sidebands is shown in Fig. 2(b), where the events primarily accumulate in the lower left corner where the momentum of pions is low.
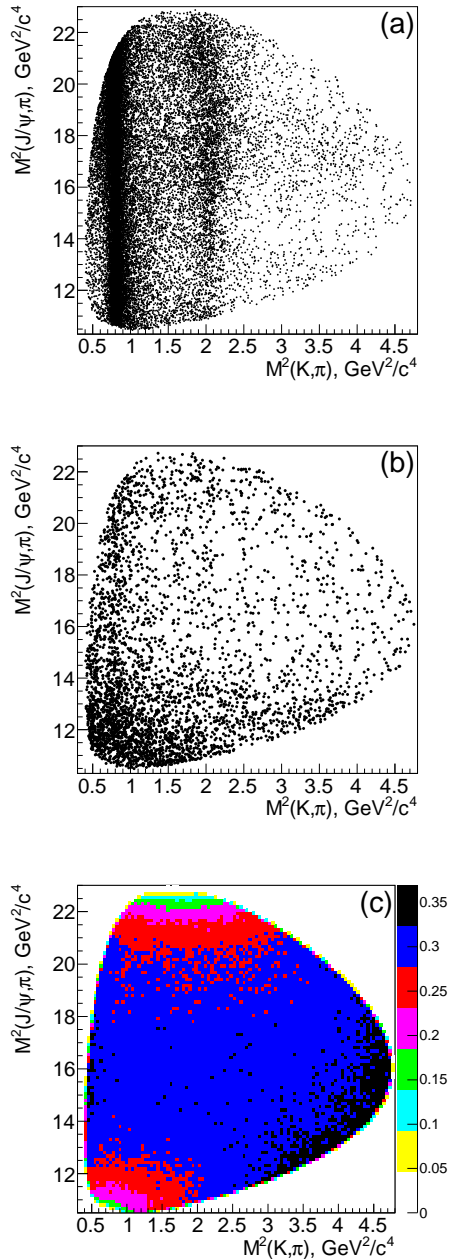

FIG. 2. Dalitz plots of the signal region (a), sidebands (b) and signal efficiency (c).

To determine the reconstruction efficiency, we generate MC events for $\bar{B}^0 \to J/\psi(\to \ell^+\ell^-)K^-\pi^+$ with a uniform phase space distribution. The efficiency is corrected for the difference between the particle identification efficiency in data and MC, which is obtained from a $D^{*+} \to D^0(\to K^-\pi^+)\pi^+$ control sample for K and π and a sample of $\gamma\gamma \to \ell^+\ell^-$ for μ and e.

The efficiency as a function of the Dalitz variables is shown in Fig. 2(c). The efficiency drops in the lower left corner where the pions have low momentum and in the upper corner where the kaons are low-momentum; elsewhere, it is almost flat. The efficiency as a function of the angular variables is shown in Fig. 3; $\theta_{J/\psi}$ is the J/ψ helicity angle, defined as the angle between the momenta of the (K^-, π^+) system and the ℓ^- in the J/ψ rest frame, and φ is the angle between the planes defined by the (ℓ^+, ℓ^-) and (K^-, π^+) momenta in the $\bar{B}^0$ rest frame. The efficiency is almost independent of $\cos\theta_{J/\psi}$; its dependence on φ is stronger, with a variation that is at the 10% level.
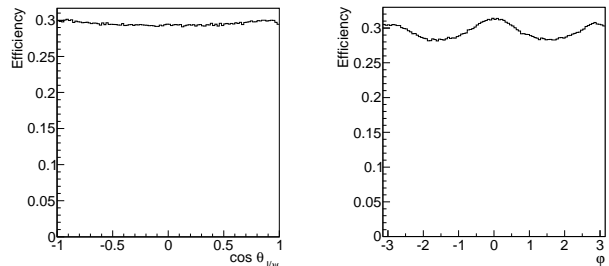

FIG. 3. Efficiency as a function of the angular variables.

V. AMPLITUDE ANALYSIS FORMALISM

The amplitude of the decay $\bar{B}^0 \to J/\psi(\to \ell^+\ell^-)K^-\pi^+$ is represented as the sum of Breit-Wigner contributions for different intermediate two-body states. The amplitude is calculated using the helicity formalism in a four-dimensional parameter space, defined as

$$\Phi = (M_{K\pi}^2, M_{J/\psi\pi}^2, \theta_{J/\psi}, \varphi). \quad (1)$$

The contributions of each individual K^* resonance and the Z_c^+ resonance to the signal density function $S(\Phi)$ are the same as in Ref. [6]; the definition of the helicity amplitudes H_λ is also the same. The difference from Ref. [6] is that the default model includes more K^* resonances due to the larger accessible kinematic range (up to $M_{K\pi} = 2183$ MeV/c^2). The known resonances included in the default model are $K_0^*(800)$, $K^*(892)$, $K^*(1410)$, $K_0^*(1430)$, $K_2^*(1430)$, $K^*(1680)$, $K_3^*(1780)$, $K_0^*(1950)$, $K_2^*(1980)$, $K_4^*(2045)$ and $Z_c(4430)^+$; a search for additional exotic Z_c^+ resonances is performed.

The background density function is

$$B(\Phi) = (B_{\rm sm}(\Phi) + B_{K^*}(\Phi) + B_{K_S^0}(\Phi)) \\ \times P_{\theta_{J/\psi}}(\cos\theta_{J/\psi})P_\varphi(\varphi), \quad (2)$$

where $B_{\rm sm}$ is the smooth part of the background, B_{K^*} is the background from the $K^*(892)$ mesons, $B_{K_S^0}$ is the $K_S^0 \to \pi^+\pi^-$ background (where one of the π mesons is misidentified as a K) and $P_{\theta_{J/\psi}}$ and P_{φ} are second-order polynomials.

The smooth part of the background is described by

$$B_{\rm sm}(\Phi) = (\alpha_1 e^{-\beta_1 M^2_{K^-\pi^+}} + \alpha_2 e^{-\beta_2 M^2_{J/\psi K^-}}) \quad (3)$$
$$\times P_{\rm sm}(M^2_{K\pi}, M^2_{J/\psi\pi}),$$

where α_1, α_2, β_1 and β_2 are real parameters and $P_{\rm sm}$ is a two-dimensional fifth-order polynomial. The background originating from the $K^*(892)$ mesons is described by the function

$$B_{K^*}(\Phi) = |A^{K^*(892)}(M^2_{K\pi})|^2 P_{K^*}(M^2_{J/\psi\pi}), \quad (4)$$

where $A^{K^*(892)}$ is the Breit-Wigner amplitude of the $K^*(892)$ and P_{K^*} is a fourth-order polynomial.

Background events from $K_S^0 \to \pi^+\pi^-$ decays have a specific $M^2_{K\pi}$ dependence on $M^2_{J/\psi\pi}$:

$$M^2_{K\pi}(K_S^0) = M^2_{K_S^0} + M^2_{K^+} - M^2_{\pi^+}$$
$$+ \frac{M^2_{K_S^0} + M^2_{\pi^+} - M^2_{J/\psi} + M^2_{J/\psi\pi}}{M_{B^0}} \quad (5)$$
$$\times \left(\sqrt{E_\pi^2 + M^2_{K^+} - M^2_\pi} - E_\pi \right),$$

where

$$E_\pi = \frac{M^2_{B^0} + M^2_{\pi^+} - M^2_{J/\psi\pi}}{2M_{B^0}} \quad (6)$$

is the energy of the incorrectly identified π meson. The K_S^0 background is described by the function

$$B_{K_S^0}(\Phi) = \exp\left[-\frac{(M^2_{K\pi} - M^2_{K\pi}(K_S^0))^2}{2\sigma^2} \right] P_{K_S^0}(M^2_{J/\psi\pi}), \quad (7)$$

where $P_{K_S^0}$ is a fourth-order polynomial and σ is the resolution.

All the parameters in Eq. (2) are free except α_1 and the constant terms of the polynomials $P_{\rm sm}$, P_{φ} and $P_{\theta_{J/\psi}}$, which are fixed at 1. The $B \to J/\psi K_S^0$ events are present only in the left ΔE sideband. This contribution is included in the fit of the sideband data that is performed to determine the background shape but excluded for the signal region.

We perform an unbinned maximum likelihood fit over the four-dimensional space Φ. The likelihood function is the same as in Ref. [6]. The masses and widths of all the K^* resonances except $K_0^*(800)$ are fixed to their nominal values [22]. The mass and width of the $K_0^*(800)$ are fixed to the fit results in the default model without a Z_c^+ ($M = 931 \pm 21$ MeV/c^2, $\Gamma = 578 \pm 49$ MeV); the case of free mass and width is included in the systematic uncertainty. The mass M and the width Γ of the $Z_c(4430)^+$
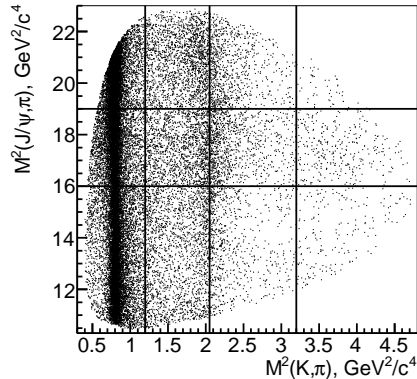

FIG. 4. Dalitz plot slices used to present results. Vertical divisions are at 1.2 GeV$^2/c^4$, $(1.432)^2$ GeV$^2/c^4$ and 3.2 GeV$^2/c^4$ (the second division is chosen to be at the $K_2^*(1430)$ mass since the interference of the K^* resonances and the $Z_c(4200)^+$ changes at this mass). Horizontal divisions are at 16 GeV$^2/c^4$ and 19 GeV$^2/c^4$.

are free parameters; however, the known mass M_0 and width Γ_0 are used to limit the floating mass and width by modifying $-2\ln L$:

$$-2\ln L \to -2\ln L + \frac{(M - M_0)^2}{\sigma^2_{M_0}} + \frac{(\Gamma - \Gamma_0)^2}{\sigma^2_{\Gamma_0}}, \quad (8)$$

where σ_{M_0} and σ_{Γ_0} are the uncertainties of M_0 and Γ_0, respectively. The values of the $Z_c(4430)^+$ mass and width are taken from Ref. [6]:

$$M_0 = 4485^{+36}_{-25} \text{ MeV}/c^2, \ \Gamma_0 = 200^{+49}_{-58} \text{ MeV}.$$

Other details of the fitting procedure are the same as in Ref. [6].

VI. RESULTS

A. Fit results

To present the fit results, the Dalitz plot is divided into the slices shown in Fig. 4. The results of the fit to the background events are shown in Fig. 5.

A search for a Z_c^+ with arbitrary mass and width is performed. The considered spin-parity hypotheses are $J^P = 0^-$, 1^-, 1^+, 2^- and 2^+. The 0^+ combination is forbidden by parity conservation in $Z_c^+ \to J/\psi\pi^+$ decays. The fit results for the Z_c^+ mass, width and significance in the default model are shown in Table I. The Wilks significance of the Z_c^+ with $J^P = 1^+$ is 8.2σ; its global significance is 7.9σ. The significance calculation method is described in Appendix A. The global significance with the systematic uncertainty is 6.2σ (the calculation is described further in this section). Thus, a new Z_c^+ state is
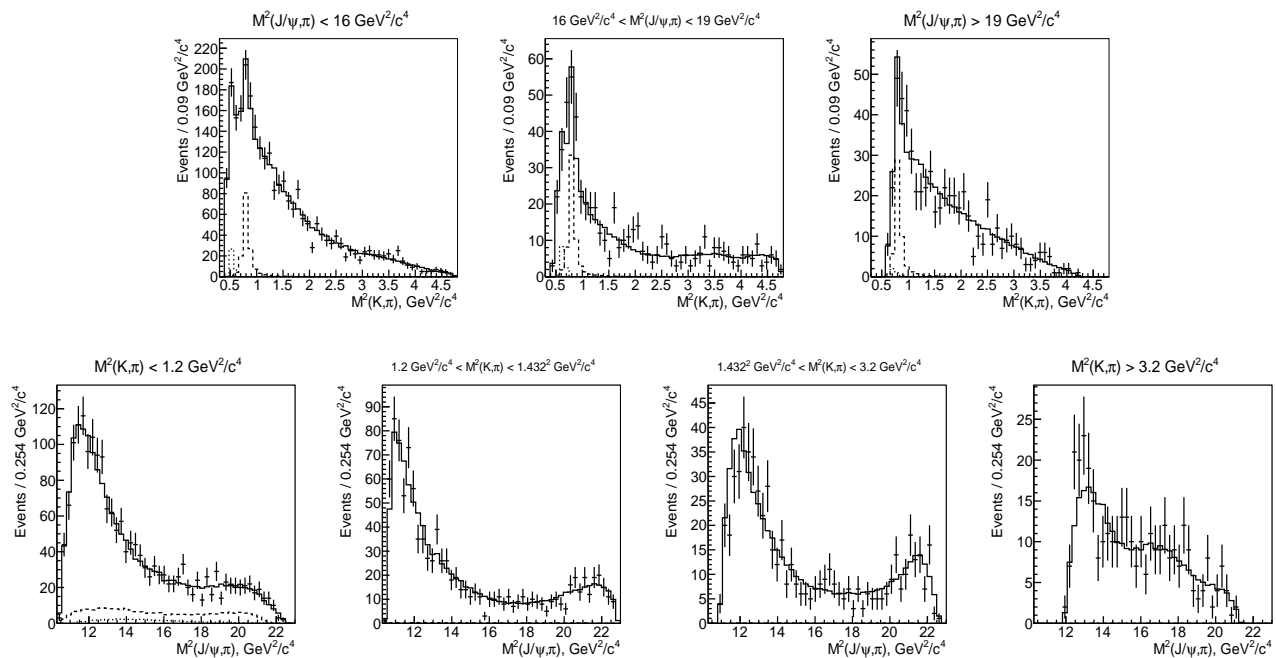
FIG. 5. Fit to the background events. The solid line is the fit result; the dashed line is the $K^*(892)$ component; the dotted line is the $K_S^0 \to \pi^+\pi^-$ component. The slices are defined in Fig. 4.

observed. In the following, this state is referred to as the $Z_c(4200)^+$. The preferred spin-parity hypothesis is 1^+. The Wilks significance of the $Z_c(4430)^+$ in the default model is 5.1σ; the global significance is found to be the same. The significance with the systematic uncertainty is 4.0σ. Thus we find evidence for a new decay channel of the $Z_c(4430)^+$.

To test the goodness of the fit, we bin the Dalitz distribution with the requirement that the number of events in each bin satisfy $n_i > 25$. We then calculate the χ^2 value as $\sum_i (n_i - s_i)^2/s_i$, where s_i is the integral of the fitting function over bin i. Since the fit is a maximum likelihood fit, we obtain the number of degrees of freedom by generating MC pseudoexperiments in accordance with the result of the fit; then, the distribution of the χ^2 value in the pseudoexperiments is fitted to the χ^2 distribution with variable number of degrees of freedom. The confidence level of the fit with the $Z_c(4200)^+$ (for the 1^+ hypothesis) is 13%; the confidence level of the fit without the $Z_c(4200)^+$ is 1.8%. We also calculate the confidence level using 4-dimensional binning (3 bins for $|\cos\theta_{J/\psi}|$ and φ and similar adaptive binning for the Dalitz plot variables); the resulting confidence level is larger. The amplitude absolute values and phases in the default model are listed in Table II. The significances of the K^* resonances are shown in Table III.

Since the $Z_c(4200)^+$ is a known resonance, before showing the fit results with and without the $Z_c(4200)^+$, we present a comparison of the fit results with and without the $Z_c(4430)^+$ with the $Z_c(4200)^+$ not included in the model, as shown in Fig. 6. There is no peak in

the $Z_c(4430)^+$ region; instead, destructive interference is seen. Projections of the fit results onto the $M_{K\pi}^2$ and $M_{J/\psi\pi}^2$ axes for the model with the $Z_c(4200)^+$ ($J^P = 1^+$) and the model without the $Z_c(4200)^+$ are shown in Fig. 7. The two peaks evident in the projections onto the $M_{K\pi}^2$ axis are due to the $K^*(892)$ and $K_2^*(1430)$ resonances. The new resonance $Z_c(4200)^+$ is seen as a wide peak near the center of the projections onto the $M_{J/\psi\pi}^2$ axis. Projections of the K^*, $Z_c(4200)^+$ and $Z_c(4430)^+$ contributions onto the $M_{J/\psi\pi}^2$ axis are shown in Fig. 8. Projections onto the angular variables for the region defined by $M_{K\pi}^2 > 1.2\,\text{GeV}^2/c^4$, $16\,\text{GeV}^2/c^4 < M_{J/\psi\pi}^2 < 19\,\text{GeV}^2/c^4$ (the intersection of the second horizontal slice and the second, third and fourth vertical slices, where the $Z_c(4200)^+$ signal is mostly concentrated) are shown in Fig. 9. Comparison of the fit results with and without the $Z_c(4430)^+$ with the $Z_c(4200)^+$ included in the model is shown in Fig. 10.

We also consider other amplitude models: without one of the insignificant K^* resonances $[K^*(1680), K_0^*(1950)]$; with the addition of S-, P- and D-wave nonresonant $K^-\pi^+$ amplitudes; with free Blatt-Weisskopf r parameters; with free masses and widths of K^* resonances (with Gaussian constraints to their known values [22]) and with the LASS amplitudes [23] instead of Breit-Wigner amplitudes for all spin-0 K^* resonances.

The significances of the $Z_c(4200)^+$ for all models other than the default are shown in Table IV. The minimal Wilks significance for the 1^+ hypotheses is 6.6σ; the corresponding global significance is 6.2σ.

TABLE I. Fit results in the default model. Errors are statistical only.

J^P	0^-	1^-	1^+	2^-	2^+
Mass, MeV/c^2	4318 ± 48	4315 ± 40	4196^{+31}_{-29}	4209 ± 14	4203 ± 24
Width, MeV	720 ± 254	220 ± 80	370 ± 70	64 ± 18	121 ± 53
Significance (Wilks)	3.9σ	2.3σ	8.2σ	3.9σ	1.9σ
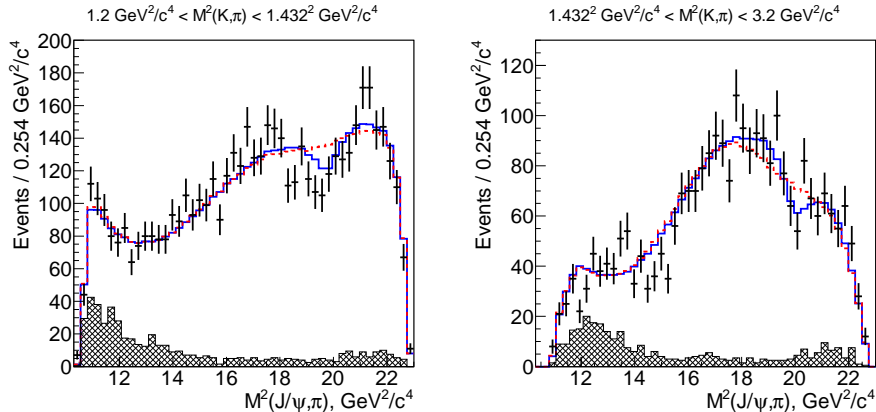
FIG. 6. The fit results with (solid line) and without (dashed line) the $Z_c(4430)^+$ (the $Z_c(4200)^+$ is not included in the model) for the second and third vertical slices that are defined in Fig. 4.

The exclusion levels of the spin-parity hypotheses ($J^P = j^p$, $j^p \in \{0^+, 1^-, 2^-, 2^+\}$) for the default model are calculated using MC simulation. The procedure is the same as in Ref. [6]. We generate MC pseudoexperiments in accordance with the fit result with the j^p $Z_c(4200)^+$ signal in data and fit them with the j^p and 1^+ signals. The resulting distribution of $\Delta(-2\ln L) = (-2\ln L)_{J^P = j^p} - (-2\ln L)_{J^P = 1^+}$ is fitted to an asymmetrical Gaussian function and the p-value is calculated as the integral of the fitting function normalized to 1 from the value of $\Delta(-2\ln L)$ in data to $+\infty$. The results are presented in Table V.

We also generate MC pseudoexperiments in accordance with the fit results for the 1^+ hypothesis, fit them with the j^p and 1^+ signals and obtain the distribution of $\Delta(-2\ln L)$. This distribution is fitted to an asymmetrical Gaussian function and the confidence level of the 1^+ hypothesis is calculated as the integral of the fitting function normalized to 1 from $-\infty$ to the value of $\Delta(-2\ln L)$ in data. The resulting confidence levels are shown in Table V. The distributions of $\Delta(-2\ln L)$ for $j^p = 2^-$ are shown in Fig. 11.

For models other than the default, we do not use the calculation of exclusion levels of the spin-parity hypotheses based on MC pseudoexperiments. Instead, the significance of the 1^+ hypothesis over the j^p hypothesis is estimated as $\sqrt{\Delta(-2\ln L)}$. The comparison of the two methods for the default model is shown in Table V. The formula-based calculation results in smaller values of the significance than the MC-based calculation, and thus it provides a conservative estimate of the significance. The results for all models are shown in Table VI. The 1^+ hypothesis is favored over the 0^-, 1^-, 2^-, 2^+ hypotheses at the levels of 6.1σ, 7.4σ, 4.4σ and 7.0σ, respectively.

The results of the study of the model dependence of the $Z_c(4200)^+$ mass and width are shown in Table VII. The maximal deviations of the mass and the width of the $Z_c(4200)^+$ from the default model values are considered as the systematic uncertainty due to the amplitude model dependence.

We also estimate the systematic error associated with the uncertainties in the modeling of the background distribution by varying the background parameters by $\pm 1\sigma$ (with other parameters varied in accordance with the correlation coefficients) and performing the fit to the data. The maximal deviations are considered as the systematic error due to the background parameterization uncertainty. This error is found to be negligibly small compared to the error due to amplitude model dependence for all the results.

Using the helicity amplitudes shown in Table II, one can calculate the amplitudes in the transversity basis:

$$A_0 = H_0, \ \ A_\parallel = \frac{H_1 + H_{-1}}{\sqrt{2}}, \ \ A_\perp = \frac{H_1 - H_{-1}}{\sqrt{2}}, \quad (9)$$

where A_0, $A_\parallel$ and $A_\perp$ are the transversity amplitudes. The amplitudes from Table II should be normalized so that, for a K^* resonance,

$$|H_0|^2 + |H_1|^2 + |H_{-1}|^2 = 1 \quad (10)$$

before the application of Eq. (9). The resulting transversity amplitudes for the $K^*(892)$ are shown in Table VIII.
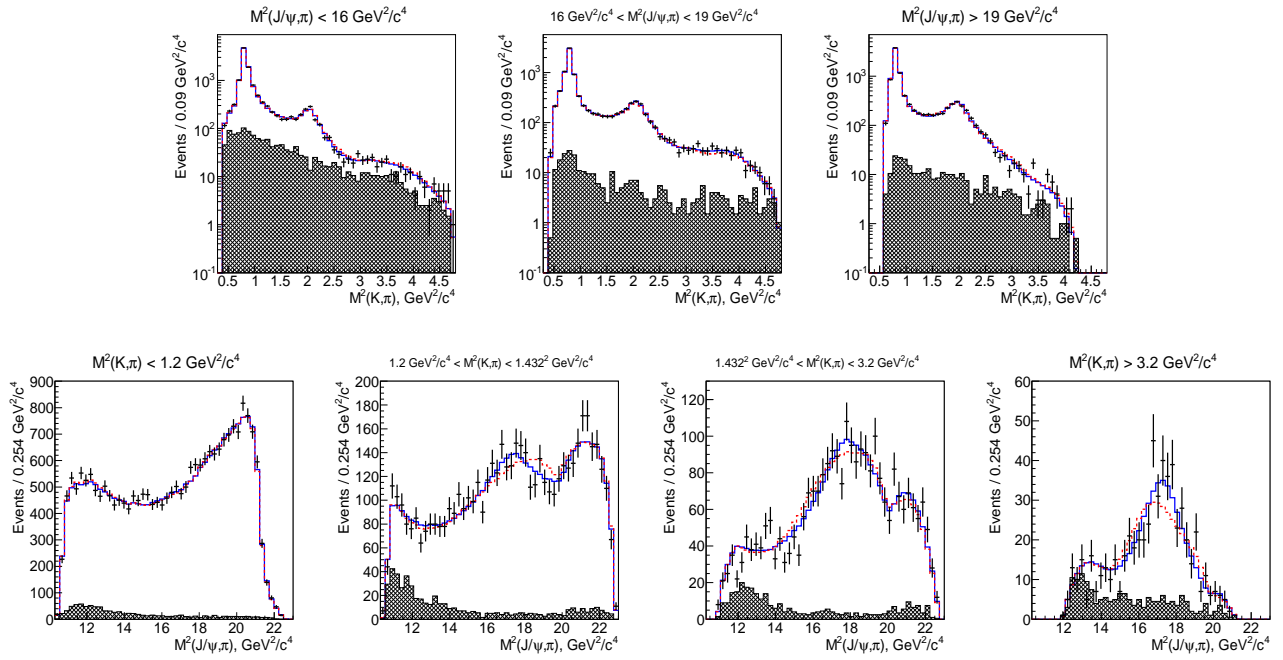
FIG. 7. The fit results with (solid line) and without (dashed line) the $Z_c(4200)^+$ ($J^P = 1^+$) in the default model. The points with error bars are data; the hatched histograms are the J/ψ sidebands. The slices are defined in Fig. 4.
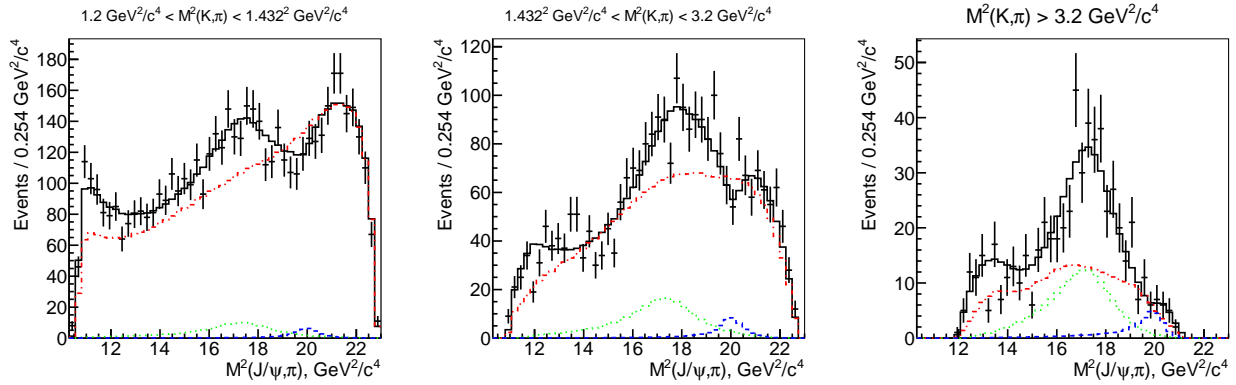

FIG. 8. The fit results with the $Z_c(4200)^+$ ($J^P = 1^+$) in the default model. The points with error bars are data; the solid histograms are fit results, the dashed histograms are the $Z_c(4430)^+$ contributions, the dotted histograms are the $Z_c(4200)^+$ contributions and the dash-dotted histograms are contributions of all K^* resonances. The slices are defined in Fig. 4.

The transversity amplitude systematic errors are due to amplitude model dependence. The results agree with previous Belle measurements for the $(B^0 + \bar{B}^0)$ sample in Ref. [24] and supersede them.

We perform a search for the $Z_c(3900)^+$, using the amplitude model with the $Z_c(4200)^+$ ($J^P = 1^+$) as a null hypothesis. All quantum number hypotheses with $J \leq 2$ are considered ($J^P \in \{0^+, 1^-, 1^+, 2^-$ and $2^+\}$). We limit the mass and the width of the $Z_c(3900)^+$ in the same way as for the $Z_c(4430)^+$. The average result of BESIII [11],

Belle [12] and analysis based on CLEO data [13].

$$M_0 = 3891.2 \pm 3.3 \text{ MeV}/c^2, \ \Gamma_0 = 39.5 \pm 8.1 \text{ MeV},$$

is used as the nominal mass and width of the $Z_c(3900)^+$. The results are shown in Table IX. No significant signal is found.

TABLE II. The absolute values and phases of the helicity amplitudes in the default model for the 1^+ spin-parity of the $Z_c(4200)^+$. Errors are statistical only.

Resonance	$|H_0|$	$\arg H_0$	$|H_1|$	$\arg H_1$	$|H_{-1}|$	$\arg H_{-1}$
$K_0^*(800)$	1.12 ± 0.04	2.30 ± 0.04	—	—	—	—
$K^*(892)$	1.0 (fixed)	0.0 (fixed)	$(8.44 \pm 0.10) \times 10^{-1}$	3.14 ± 0.03	$(1.96 \pm 0.14) \times 10^{-1}$	-1.70 ± 0.07
$K^*(1410)$	$(1.19 \pm 0.27) \times 10^{-1}$	0.81 ± 0.26	$(1.23 \pm 0.38) \times 10^{-1}$	-1.04 ± 0.26	$(0.36 \pm 0.39) \times 10^{-1}$	0.67 ± 1.06
$K_0^*(1430)$	$(8.90 \pm 0.28) \times 10^{-1}$	-2.17 ± 0.05	—	—	—	—
$K_2^*(1430)$	4.66 ± 0.18	-0.32 ± 0.05	4.65 ± 0.18	-3.05 ± 0.08	1.26 ± 0.23	-1.92 ± 0.20
$K^*(1680)$	$(1.39 \pm 0.43) \times 10^{-1}$	-2.46 ± 0.31	$(0.82 \pm 0.48) \times 10^{-1}$	-2.85 ± 0.49	$(1.61 \pm 0.56) \times 10^{-1}$	1.88 ± 0.28
$K_3^*(1780)$	16.8 ± 3.6	-1.43 ± 0.24	19.1 ± 4.5	2.03 ± 0.31	10.2 ± 5.2	1.55 ± 0.62
$K_0^*(1950)$	$(2.41 \pm 0.60) \times 10^{-1}$	-2.39 ± 0.25	—	—	—	—
$K_2^*(1980)$	4.53 ± 0.74	-0.26 ± 0.16	3.78 ± 0.98	3.08 ± 0.28	3.51 ± 1.03	2.63 ± 0.34
$K_4^*(2045)$	590 ± 136	-2.66 ± 0.23	676 ± 164	0.06 ± 0.25	103 ± 174	-1.03 ± 1.62
$Z_c(4430)^+$	1.12 ± 0.32	-0.31 ± 0.26	1.17 ± 0.46	0.77 ± 0.25	$H_{-1} = H_1$	
$Z_c(4200)^+$	0.71 ± 0.37	2.14 ± 0.40	3.23 ± 0.79	3.00 ± 0.15	$H_{-1} = H_1$	

TABLE III. The fit fractions and significances of all resonances in the default model ($J^P = 1^+$).

Resonance	Fit fraction	Significance (Wilks)
$K_0^*(800)$	$(7.1^{+0.7}_{-0.5})\%$	22.5σ
$K^*(892)$	$(69.0^{+0.6}_{-0.5})\%$	166.4σ
$K^*(1410)$	$(0.3^{+0.2}_{-0.1})\%$	4.1σ
$K_0^*(1430)$	$(5.9^{+0.6}_{-0.4})\%$	22.0σ
$K_2^*(1430)$	$(6.3^{+0.3}_{-0.4})\%$	23.5σ
$K^*(1680)$	$(0.3^{+0.2}_{-0.1})\%$	2.7σ
$K_3^*(1780)$	$(0.2^{+0.1}_{-0.1})\%$	3.8σ
$K_0^*(1950)$	$(0.1^{+0.1}_{-0.1})\%$	1.2σ
$K_2^*(1980)$	$(0.4^{+0.1}_{-0.1})\%$	5.3σ
$K_4^*(2045)$	$(0.2^{+0.1}_{-0.1})\%$	3.8σ
$Z_c(4430)^+$	$(0.5^{+0.4}_{-0.1})\%$	5.1σ
$Z_c(4200)^+$	$(1.9^{+0.7}_{-0.5})\%$	8.2σ

B. Efficiency and branching fractions

We use the signal density function determined from the fits to calculate the efficiency

$$\epsilon_0 = \frac{\int S(\Phi)\epsilon(\Phi)d\Phi}{\int S(\Phi)d\Phi}, \qquad (11)$$

where $\epsilon(\Phi)$ is the phase-space-dependent efficiency. The reconstruction efficiency is found to be $\epsilon_0 = (28.4 \pm 1.1)\%$. The central value is calculated for the default model with Z_c^+ ($J^P = 1^+$). The efficiency includes the correction for the difference between the particle identification efficiency in MC and data, $(93.1 \pm 3.5)\%$. The relative error of the efficiency includes the uncertainty in track reconstruction efficiency (1.4%), the error from the particle identification efficiency difference between MC and data (3.8%) and the uncertainty due to the amplitude model

TABLE IV. Model dependence of the $Z_c(4200)^+$ Wilks significance.

Model	0^-	1^-	1^+	2^-	2^+
Without $K^*(1680)$	3.2σ	3.1σ	8.4σ	3.7σ	1.9σ
Without $K_0^*(1950)$	3.6σ	2.8σ	8.6σ	5.0σ	2.6σ
LASS	3.8σ	1.0σ	6.6σ	5.2σ	2.3σ
Free masses and widths	2.4σ	1.6σ	7.3σ	4.6σ	1.9σ
Free r	5.0σ	2.6σ	8.4σ	4.5σ	0.9σ
Nonresonant ampl. (S)	3.8σ	2.9σ	7.9σ	4.1σ	2.0σ
Nonresonant ampl. (S,P)	3.7σ	2.4σ	7.7σ	3.7σ	1.4σ
Nonresonant ampl. (S,P,D)	4.1σ	2.3σ	7.7σ	3.8σ	1.3σ

TABLE V. Exclusion levels of the $Z_c(4200)^+$ spin-parity hypotheses and confidence levels of the 1^+ hypothesis for the default model.

j^p	1^+ over j^p		1^+ C. L.
	MC	$\sqrt{\Delta(-2\ln L)}$	
0^-	8.6σ	7.9σ	26%
1^-	9.8σ	8.7σ	48%
2^-	8.8σ	7.6σ	40%
2^+	10.6σ	8.8σ	42%

TABLE VI. Exclusion levels of the $Z_c(4200)^+$ spin-parity hypotheses.

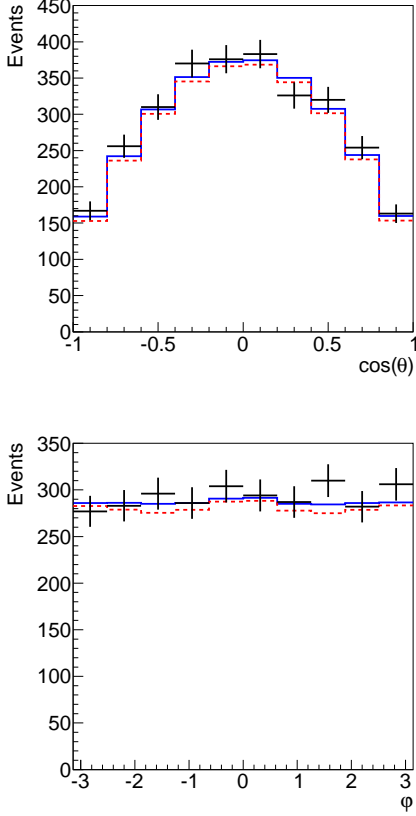| Model	0^-	1^-	2^-	2^+
Without $K^*(1680)$	8.5σ	8.5σ	8.0σ	9.0σ
Without $K_0^*(1950)$	8.4σ	8.8σ	7.3σ	8.9σ
LASS	6.1σ	7.4σ	4.4σ	7.0σ
Free masses and widths	7.6σ	7.9σ	5.9σ	7.8σ
Free r	7.4σ	8.7σ	7.5σ	9.2σ
Nonresonant ampl. (S)	7.6σ	8.1σ	7.2σ	8.5σ
Nonresonant ampl. (S,P)	7.4σ	8.1σ	7.2σ	8.4σ
Nonresonant ampl. (S,P,D)	7.2σ	8.1σ	7.1σ	8.4σ

FIG. 9. Projections of the fit results with (solid line) and without (dashed line) the $Z_c(4200)^+$ ($J^P = 1^+$) onto the angular variables in the default model for the region defined by $M_{K\pi}^2 > 1.2\,\mathrm{GeV}^2/c^4$, $16\,\mathrm{GeV}^2/c^4 < M_{J/\psi\pi}^2 < 19\,\mathrm{GeV}^2/c^4$. Points with error bars are data.

TABLE VII. Systematic uncertainties in the $Z_c(4200)^+$ mass (in MeV/c^2) and width (in MeV).

Model or error source	Mass	Width
Without $K^*(1680)$	$^{+0}_{-1}$	$^{+0}_{-34}$
Without $K_0^*(1950)$	$^{+9}_{-0}$	$^{+0}_{-54}$
LASS	$^{+0}_{-13}$	$^{+0}_{-132}$
Free masses and widths	$^{+0}_{-3}$	$^{+0}_{-29}$
Free r	$^{+16}_{-0}$	$^{+58}_{-0}$
Nonresonant ampl. (S)	$^{+0}_{-6}$	$^{+0}_{-15}$
Nonresonant ampl. (S,P)	$^{+17}_{-0}$	$^{+70}_{-0}$
Nonresonant ampl. (S,P,D)	$^{+0}_{-0}$	$^{+6}_{-0}$
Amplitude model, total	$^{+17}_{-13}$	$^{+70}_{-132}$

dependence (0.3%). The error due to MC statistics is negligibly small.

Using the obtained efficiency and the branching fractions for J/ψ decays to e^+e^- and $\mu^+\mu^-$ [22], we deter-

TABLE VIII. The transversity amplitudes of the $K^*(892)$.

Parameter	Result
$|A_\parallel|^2$	$0.227 \pm 0.007 \pm 0.006$
$|A_\perp|^2$	$0.201 \pm 0.007 \pm 0.005$
$\arg A_\parallel$	$-2.92 \pm 0.04 \pm 0.04$
$\arg A_\perp$	$2.91 \pm 0.03 \pm 0.03$

mine:

$$\mathcal{B}(\bar{B}^0 \to J/\psi K^-\pi^+) = (1.15 \pm 0.01 \pm 0.05) \times 10^{-3}.$$

This result assumes equal production of $B^0\bar{B}^0$ and B^+B^- pairs. The central value is given for the default model with the $J^P = 1^+$ assignment for the $Z_c(4200)^+$. The systematic error includes the uncertainty in the efficiency, the number of B mesons (1.4%), the signal yield (0.3%) and the $J/\psi \to \ell^+\ell^-$ branching fraction (1.0%).

The fit fraction of a resonance R [the $Z_c(4200)^+$, $Z_c(4430)^+$ or one of the K^* resonances] is defined as

$$f = \frac{\int S_R(\Phi)d\Phi}{\int S(\Phi)d\Phi}, \tag{12}$$

where $S_R(\Phi)$ is the signal density function with all contributions other than the contribution of the R resonance set to 0. The statistical uncertainties in the fit fractions are determined from a set of MC pseudoexperiments generated in accordance with the fit result in data. We fit each sample and calculate the fit fractions; the resulting distribution of the fit fractions is fitted to an asymmetric Gaussian function with peak position fixed at the fit fraction in data. The standard deviations of the Gaussian function are treated as the statistical uncertainties. We find good agreement between the distributions of the fit fractions in the pseudoexperiments with the fitting function for all resonances except the $K^*(892)$. For the $K^*(892)$, we release the peak position and treat the difference between the resulting fit fraction and the fit fraction in data (-0.42% absolute or -0.61% relative) as an additional systematic error due to fit bias. The results are summarized in Table III.

The branching fraction of $B^0 \to J/\psi K^*(892)$ decay is given by

$$\begin{aligned}\mathcal{B}(\bar{B}^0 \to J/\psi K^*(892)) = \\ 1.5\, f_{K^*(892)}\, \mathcal{B}(\bar{B}^0 \to J/\psi K^-\pi^+),\end{aligned} \tag{13}$$

where $f_{K^*(892)}$ is the fit fraction of the $K^*(892)$. The result is

$$\mathcal{B}(\bar{B}^0 \to J/\psi K^*(892)) = (1.19 \pm 0.01 \pm 0.08) \times 10^{-3}.$$

The systematic error includes contributions from the same sources as the uncertainty in the branching fraction of $\bar{B}^0 \to J/\psi K^-\pi^+$ decay, fit bias for the $K^*(892)$ fit fraction (-0.6%) and the amplitude model $[(^{+1.5}_{-2.0})\%]$ dependence of the $K^*(892)$ fit fraction.
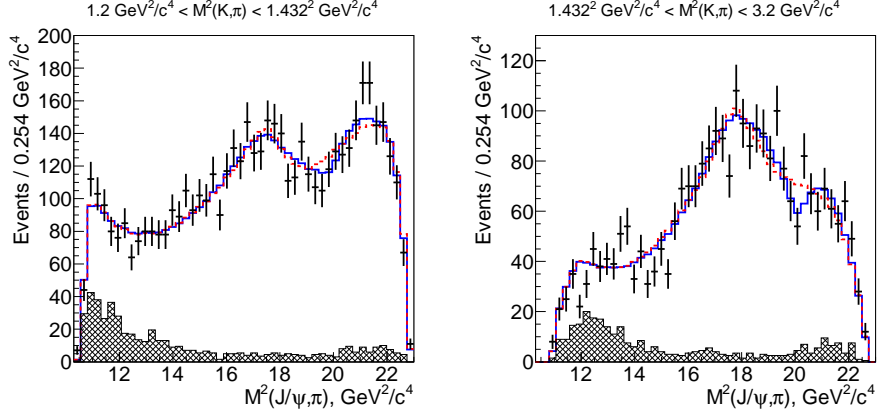
FIG. 10. The fit results with (solid line) and without (dashed line) the $Z_c(4430)^+$ (the $Z_c(4200)^+$ is included in the model) for the second and third vertical slices that are defined in Fig. 4.

TABLE IX. Fit results with addition of the $Z_c(3900)^+$ in the default model. Errors are statistical only.

J^P	0^-	1^-	1^+	2^-	2^+
Mass, MeV/c^2	3889.8 ± 3.3	3890.3 ± 3.1	3890.6 ± 3.3	3891.1 ± 3.2	3891.5 ± 3.3
Width, MeV	43.2 ± 6.5	37.8 ± 7.9	39.2 ± 8.1	39.4 ± 8.5	41.2 ± 7.7
Significance	2.4σ	1.1σ	0.1σ	$< 0.1\sigma$	0.2σ
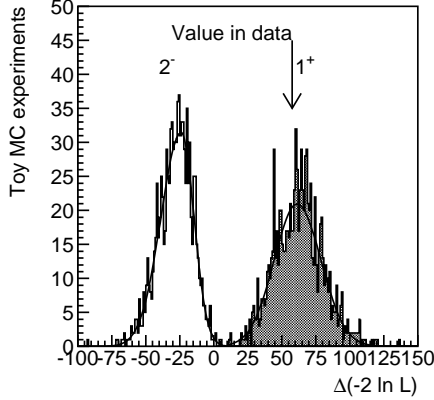
FIG. 11. Comparison of the 2^- and 1^+ hypotheses in the default model. The histograms are distributions of $\Delta(-2\ln L)$ in MC pseudoexperiments generated in accordance with the fit results with 2^- (open histogram) and 1^+ (hatched histogram) Z_c^+ signals. The $\Delta(-2\ln L)$ value observed in data is indicated with an arrow.

The branching fraction products for the $Z_c(4430)^+$ and $Z_c(4200)^+$ are

$$\mathcal{B}(\bar{B}^0 \to Z_c(4430)^+ K^-) \times \mathcal{B}(Z_c(4430)^+ \to J/\psi\pi^+) =$$
$$(5.4^{+4.0+1.1}_{-1.0-0.9}) \times 10^{-6},$$
$$\mathcal{B}(\bar{B}^0 \to Z_c(4200)^+ K^-) \times \mathcal{B}(Z_c(4200)^+ \to J/\psi\pi^+) =$$
$$(2.2^{+0.7+1.1}_{-0.5-0.6}) \times 10^{-5},$$

where the systematic error due to the amplitude model dependence is $(^{+19.9}_{-14.9})\%$ and $(^{+49.0}_{-26.7})\%$, respectively.

To calculate the upper limit of the branching fraction product for the $Z_c(3900)^+$, its quantum numbers are assumed to be $J^P = 1^+$ in accordance with the result of BESIII angular analysis in the $D\bar{D}^*$ decay mode [14]. The result is

$$\mathcal{B}(\bar{B}^0 \to Z_c(3900)^+ K^-) \times \mathcal{B}(Z_c(3900)^+ \to J/\psi\pi^+) <$$
$$9 \times 10^{-7} \ (90\% \ \text{CL}).$$

VII. CONCLUSIONS

An amplitude analysis of $\bar{B}^0 \to J/\psi K^- \pi^+$ decays in four dimensions has been performed. A new charged charmonium-like state $Z_c(4200)^+$ decaying to J/ψ and π^+ is observed with the significance of 6.2σ. The minimal quark content of this state is exotic: $|c\bar{c}u\bar{d}\rangle$. Its mass and width are measured to be

$$M = 4196^{+31+17}_{-29-13} \ \text{MeV}/c^2,$$
$$\Gamma = 370^{+70+70}_{-70-132} \ \text{MeV}.$$

The preferred quantum number assignment is $J^P = 1^+$. Other hypotheses with $J^P \in \{0^-, 1^-, 2^-, 2^+\}$ are excluded at the levels of 6.1σ, 7.4σ, 4.4σ and 7.0σ, respectively. Also, evidence for a new decay channel $\to J/\psi\pi^+$ of the $Z_c(4430)^+$ is found.

The LHCb Collaboration included a second Z_c^+ state in the amplitude analysis of $\bar{B}^0 \to \psi(2S)K^-\pi^+$ decays

together with the $Z_c(4430)^+$, but did not claim an observation [10]. The reported mass and width of this second Z_c^+ are close to the mass and width of the $Z_c(4200)^+$ and, while the preferred quantum number assignment of the quantum numbers is $J^P = 0^-$, $J^P = 1^+$ is not excluded. Thus, the effect observed in Ref. [10] may be due to $Z_c(4200)^+ \to \psi(2S)\pi^+$.

The branching fractions are found to be

$$\mathcal{B}(\bar{B}^0 \to J/\psi K^- \pi^+) = (1.15 \pm 0.01 \pm 0.05) \times 10^{-3},$$

$$\mathcal{B}(\bar{B}^0 \to J/\psi K^*(892)) = (1.19 \pm 0.01 \pm 0.08) \times 10^{-3},$$

$$\mathcal{B}(\bar{B}^0 \to Z_c(4430)^+ K^-) \times \mathcal{B}(Z_c(4430)^+ \to J/\psi\pi^+) =$$
$$(5.4^{+4.0+1.1}_{-1.0-0.9}) \times 10^{-6},$$

$$\mathcal{B}(\bar{B}^0 \to Z_c(4200)^+ K^-) \times \mathcal{B}(Z_c(4200)^+ \to J/\psi\pi^+) =$$
$$(2.2^{+0.7+1.1}_{-0.5-0.6}) \times 10^{-5},$$

$$\mathcal{B}(\bar{B}^0 \to Z_c(3900)^+ K^-) \times \mathcal{B}(Z_c(3900)^+ \to J/\psi\pi^+) <$$
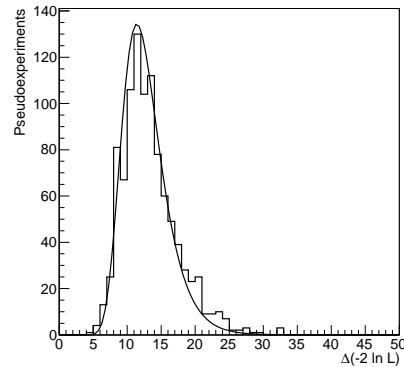$$9 \times 10^{-7} \text{ (90\% CL)}.$$

VIII. ACKNOWLEDGMENTS

FIG. 12. Results of a fit to a $\Delta(-2\ln L)$ distribution done as part of the $Z_c(4200)^+$ global significance calculation for the $J^P = 1^+$ hypothesis.

Appendix A: Calculation of the local, Wilks and global significance

For the significance calculation, one needs to know the distribution of the difference between the $-2\ln L$ values with and without a Z_c^+ contribution provided that there is no Z_c^+ signal. The Wilks significance is given by Wilks' theorem [25]:

$$p(\delta) = \int_{\delta}^{+\infty} \chi_\kappa^2(x)dx = \frac{\Gamma(\frac{\kappa}{2}, \delta/2)}{\Gamma(\frac{\kappa}{2})}, \quad (A1)$$

where $p(\delta)$ is the probability that $\Delta(-2\ln L) > \delta$; κ is the number of degrees of freedom of the χ^2 distribution, which is equal to the number of additional free parameters and $\Gamma(\kappa/2, \delta/2)$ is the upper incomplete gamma function $[\Gamma(a,x) = \int_x^{+\infty} t^{a-1}e^{-t}dt]$. In this analysis, the number of additional free parameters is four for $J^P = 0^-$, 1^- and 2^+ or six for $J^P = 1^+$ and 2^-. These parameters include mass, width and one or two complex amplitudes. The local significance is the significance with fixed mass and width; it is given by Eq. (A1) with $\kappa \to \kappa - 2$.

The mass and the width of the resonance are defined only under an alternative (*i.e.*, when amplitudes are not equal to 0), thus the real distribution of $\Delta(-2\ln L)$ may deviate from the prediction of Wilks' theorem. Further-

more, since the search is performed over two variables, the one-dimensional upcrossing method [26] is not valid.

For large values of δ, the p-value is the same as the expectation of the Euler characteristic of the excursion set [27]. This expectation $E(\delta)$ is given in Ref. [28] [Eq. (15.10.1) and Theorem 15.10.1]; it has the form

$$E(\delta) = \sum_{j=0}^{n-k} \sum_{l=0}^{\lfloor \frac{j-1}{2} \rfloor} \sum_{m=0}^{j-1-2l} C_{jml} \delta^{(k-j)/2+m+l} e^{-\delta/2}, \quad \text{(A2)}$$

where $n - k$ is the dimension, k is the number of degrees of freedom (for the application in question, n is the total number of additional free parameters and $n - k$ is equal to the number of additional free parameters defined only under alternative), $\lfloor \rfloor$ is the floor function (the largest integer that is not greater than the argument) and C_{jml} are constants. The contribution with the largest power of δ corresponds to $m = j - 1$, $l = 0$, $j = n - k$:

$$E(\delta) \sim \delta^{\frac{n}{2}-1} e^{-\delta/2}. \quad \text{(A3)}$$

In Ref. [10], the global significance is calculated by fitting the distribution of $\Delta(-2 \ln L)$ to the χ^2_κ distribution with variable number of degrees of freedom κ. The p-value is then given by Eq. (A1); for large δ, it is approximately equal to

$$p(\delta) \approx \frac{(\delta/2)^{\frac{\kappa}{2}-1} e^{-\delta/2}}{\Gamma(\frac{\kappa}{2})}. \quad \text{(A4)}$$

This only coincides with the expected tail distribution of $\Delta(-2 \ln L)$ that is given by Eq. (A3) when $\kappa = n$, $i.e.$, if there is no look-elsewhere effect. We follow the general idea of Ref. [10] of calculation of the global significance from the fit to the $\Delta(-2 \ln L)$ distribution, but construct another probability density function that agrees with Eq. (A3).

The probability density function is constructed as a generalization of a particular case of a search of a one-bin peak in a histogram with N bins with known distribution and normalization. The p-value in a particular bin is given by Eq. (A1) with $\kappa = 1$. The p-value for the entire histogram is

$$p(\delta) = 1 - \left(1 - \int_\delta^{+\infty} \chi^2_\kappa(x) dx\right)^N, \quad \text{(A5)}$$

and the corresponding distribution of $\Delta(-2 \ln L)$, which is obtained by differentiation of Eq. (A5), is

$$f(\Delta) = N \left(1 - \int_\Delta^{+\infty} \chi^2_\kappa(x) dx\right)^{N-1} \chi^2_\kappa(\Delta). \quad \text{(A6)}$$

For large Δ, this is approximately equal to

$$f(\Delta) \approx N \frac{\Delta^{\frac{\kappa}{2}-1} e^{-\Delta/2}}{2^{\frac{\kappa}{2}} \Gamma(\frac{\kappa}{2})}, \quad \text{(A7)}$$

thus

$$p(\delta) \sim \delta^{\frac{\kappa}{2}-1} e^{-\delta/2}. \quad \text{(A8)}$$

If κ is equal to the number of additional free parameters n, then Eq. (A3) holds for $p(\delta)$. The distribution of $\Delta(-2 \ln L)$ is fitted to the function

$$g(\Delta) = CN \left(1 - \int_\Delta^{+\infty} \chi^2_n(x) dx\right)^{N-1} \chi^2_n(\Delta). \quad \text{(A9)}$$

where C and N are fit parameters. The result for the search of a Z_c^+ with $J^P = 1^+$ is shown in Fig. 12; the parameter N is found to be 12.1 ± 0.4.

[1] S. Godfrey and S. L. Olsen, Ann. Rev. Nucl. Part. Sci. **58**, 51 (2008).
[2] N. Brambilla *et al.*, Eur. Phys. J. C **71**, 1534 (2011).
[3] N. Brambilla *et al.*, arXiv:1404.3723 [hep-ph].
[4] S. K. Choi *et al.* (Belle Collaboration), Phys. Rev. Lett. **100**, 142001 (2008).
[5] R. Mizuk *et al.* (Belle Collaboration), Phys. Rev. D **80**, 031104(R) (2009).
[6] K. Chilikin *et al.* (Belle Collaboration), Phys. Rev. D **88**, 074026 (2013).
[7] R. Mizuk *et al.* (Belle Collaboration), Phys. Rev. D **78**, 072004 (2008).
[8] B. Aubert *et al.* (BaBar Collaboration), Phys. Rev. D **79**, 112001 (2009).
[9] J. P. Lees *et al.* (BaBar Collaboration), Phys. Rev. D **85**, 052003 (2012).
[10] R. Aaij *et al.* (LHCb Collaboration), Phys. Rev. Lett. **112**, 222002 (2014).
[11] M. Ablikim *et al.* (BESIII Collaboration), Phys. Rev. Lett. **110**, 252001 (2013).
[12] Z. Q. Liu *et al.* (Belle Collaboration), Phys. Rev. Lett. **110**, 252002 (2013).
[13] T. Xiao, S. Dobbs, A. Tomaradze and K. K. Seth, Phys. Lett. B **727**, 366 (2013).
[14] M. Ablikim *et al.* (BESIII Collaboration), Phys. Rev. Lett. **112**, 022001 (2014).
[15] M. Ablikim *et al.* (BESIII Collaboration), Phys. Rev. Lett. **112**, 132001 (2014).
[16] M. Ablikim *et al.* (BESIII Collaboration), Phys. Rev. Lett. **111**, 242001, (2013).
[17] S. Kurokawa and E. Kikutani, Nucl. Instrum. Methods Phys. Res. Sect. A **499**, 1 (2003), and other papers included in this Volume; T. Abe *et al.*, Prog. Theor. Exp. Phys. **2013**, 03A001 (2013) and following articles up to 03A011.
[18] A. Abashian *et al.* (Belle Collaboration), Nucl. Instrum.

Methods Phys. Res. Sect. A **479**, 117 (2002); also see detector section in J. Brodzicka *et al.*, Prog. Theor. Exp. Phys. **2012**, 04D001 (2012).

[19] Z. Natkaniec *et al.* (Belle SVD2 Group), Nucl. Instrum. Methods Phys. Res. Sect. A **560**, 1 (2006).

[20] R. Brun *et al.*, GEANT 3.21, CERN DD/EE/84-1, 1984.

[21] D. J. Lange, Nucl. Instrum. Methods A **462**, 152 (2001).

[22] J. Beringer *et al.* (Particle Data Group), Phys. Rev. D **86**, 010001 (2012).

[23] D. Aston *et al.*, Nucl. Phys. B **296**, 493 (1988).

[24] R. Itoh *et al.* (Belle Collaboration), Phys. Rev. Lett. **95**, 091601 (2005).

[25] S. S. Wilks, Ann. Math. Statist. **9**, 60 (1938).

[26] E. Gross and O. Vitells, Eur. Phys. J. C **70**, 525 (2010).

[27] O. Vitells and E. Gross, Astropart. Phys. **35**, 230 (2011).

[28] R. J. Adler and J. E. Taylor, *Random fields and geometry*, Springer Monographs in Mathematics (2007). ISBN: 978-0-387-48112-8.